Vietnam Journal of Science and Technology ***62*** *(5) (2024)*

doi:10.15625/2525-2518/20460

Preparation of cobalt-modified montmorillonite for corrosion inhibition of 2024 - T3 aluminium alloy surface

Thai Thu Thuy*, Pham Gia Vu, Trinh Anh Truc

Institute for Tropical Technology, Vietnam Academy of Science and Technology, 18 Hoang Quoc Viet, Cau Giay, Ha Noi, Viet Nam

*Emails: *ttthuy@itt.vast.vn*

Received: 29 March 2024; Accepted for publication: 24 July 2024

Abstract. In this study, cobalt Co(II) cations were incorporated into the interlayer spaces of the montmorillonite matrix via a cation-exchange reaction, leading to an increase in layer spacing as Na was replaced by Co, as demonstrated by x-ray diffraction analysis. It was observed that Co could be released from the MMTCo matrix into the aqueous medium, with this release being more pronounced in alkaline environments. Electrochemical impedance spectroscopy (EIS) confirmed that MMTCo acts as an effective corrosion inhibitor for the AA2024 surface, with its inhibitive efficiency being concentration-dependent and more significant at higher concentrations. FE-SEM imaging revealed that a protective layer formed on the AA2024 surface immersed in a filtrate containing MMTCo, in contrast to surfaces exposed to the filtrate of MMT, which were significantly attacked.

Keywords: Co-modified montmorillonite, inhibition corrosion, aluminium alloy.

Classification numbers: 2.5.3, 2.10.2, 2.10.3.

1. INTRODUCTION

Inhibitors are incorporated into coatings to provide “active” protection, slowing down corrosion at coating defects. However, directly introducing corrosion inhibitors during the coating manufacturing process often leads to issues such as too rapid a release of inhibitors, which is difficult to control [1], and this can result in the formation of defects. Additionally, the inhibitor content is sometimes limited by its solubility and compatibility within the coating [2]. To address these issues, one widely used method involves using carriers that act as reservoirs for the corrosion inhibitors in the coating. Common carriers include ZrO_2 [3], TiO_2 [4], CeO_2 [5, 6], SiO_2 [7] and nanoclay [8-11]. When dispersed in the polymer matrix, they simultaneously enhance the mechanical and inhibitive properties of the coating. Nanoparticles in sheet form, such as nanoclay (sodium montmorillonite, MMTNa), are also widely used to increase the shielding ability of polymer composite materials. The chemical structure of MMTNa consists of two fused silica tetrahedral sheets sandwiching an edge-shared octahedral sheet of either magnesium or aluminum hydroxide. Na^+ ions present in the interlayer regions can be replaced

by cations such as cerium ions through a cation-exchange reaction. By incorporating cerium-modified montmorillonite (MMTCe) into an organic coating, it can serve as a pigment that enhances both the barrier and inhibitive properties of the coating [10 - 12]. The researches have also demonstrated that the incorporation of cerium-modified montmorillonite provides "active" protection for a sol-gel coating on 2024 aluminum alloy [11]. This is attributed to the leaching of cerium ions from the montmorillonite platelets at a rate of 70 % into the corrosive environment, significantly improving the protective ability of the sol-gel layer. The accelerated salt mist testing on test samples with artificial incisions has demonstrated the self-repairing ability of the cerium ions, leading to the formation of cerium hydroxide at the film/metal substrate boundary and thereby reinforcing the corrosion protection of the coating.

Cobalt salts are considered effective corrosion inhibitors for metals due to the existence of multiple oxidation states (Co^{2+}, Co^{3+}, and Co^{4+}) and the fact that the redox potential of the Co^{3+}/Co^{2+} pair (+1.92V) is close to that of the Cr^{6+}/Cr^{3+} pair (+1.36 V) in acidic environments, making Co(III) a potential oxidizing agent [13]. The high solubility of cobalt salts, however, can lead to the defect formation when formulated in paint. Therefore, cobalt cations are often attached into an inorganic compound, such as a silica or ferrite matrix. As a result, the leaching of cobalt cations can be controlled when the coating was damaged with the appearance of defects.

In the present work, cobalt cations were inserting into platelets of the MMTNa matrix by a cation-exchange reaction. The inhibitive property of cobalt modified montmorillonite (MMTCo) for corrosion protection of aluminum alloy was characterized by electrochemical method.

2. MATERIALS AND METHODS

2.1. Materials

The aluminum alloy used is the 2024-T3 type (AA2024-T3). For the electrochemical measurements, a cylindrical AA2024 bar with a 1 cm^2 surface area was carefully polished using SiC paper from 100 to 1200 grade. It was then washed with absolute ethanol, rapidly dried, and immediately submerged in the solution under study.

Sodium montmorillonite (MMTNa) is Cloisite 116® Na (BYK – Southern Clay product). Cobalt-modified montmorillonite (MMTCo) is prepared through a cation-exchange reaction [11], as described below: MMTNa (3.0 g) was dispersed in distilled water (300 mL) using ultrasonication (15W, 30 minutes). The mixture was then stirred continuously at room temperature for 24 hours to achieve a homogeneous suspension. A solution of $Co(NO_3)_2$ (98 %, Sigma Aldrich) was gradually added to this MMTNa solution (MMTNa/Co = 10/1 wt.%), and the mixture was constantly stirred at 70 °C for 24 hours. The resulting MMTCo powder was collected using a high-speed centrifuge (5000 rpm) and washed repeatedly with distilled water to remove all excess ions. Finally, the MMTCo powder was dried in a vacuum oven at 80 °C for 48 hours.

2.2. Methods

The crystallization of the synthesized MMTCo was characterized by X-ray diffraction (XRD) analysis, utilizing a Siemens D5000 diffractometer equipped with Cu Kα radiation.

The release of Co cations from MMTCo particles was effectuated in both neutral and alkaline media, and it was quantified based on the Co concentration in the filtrate. This

measurement was taken during the immersion of MMTCo in the solution under study, using UV-Vis spectroscopy Libra 80 (Biochrom). The alkaline medium was prepared using a borate buffer solution to maintain a stable pH value of 9. The deviation standard of this method was approximately 3 %, as reported in previous work [11].

Electrochemical impedance spectroscopy (EIS) measurements were performed using a three-electrode standard setup. The working electrode was the rod of AA2024 (1 cm^2 of surface area), a saturated Ag/AgCl/KCl electrode served as the reference electrode, and a platinum grid was used as the counter electrode. The EIS measurements were conducted over a frequency range from 100 kHz to 10 mHz at the open circuit potential (OCP), with an amplitude of 10 mV. Surface observation of AA2024 specimen after immersion time was examined with Thermal Field Emission Scanning Electron Microscopy JEOL JSM-IT800SHL.

Anodic and cathodic polarizations were separately obtained at a rate of 0.167 mV/s, starting from the OCP. The electrolyte solution was an aqueous solution of 0.05 M NaCl mixing 0.1 M Na_2SO_4 solution. Both the EIS and polarization measurements were conducted using Biologic SP-300 equipment. To ensure the reproducibility of the measurements, each sample was tested at least three times.

3. RESULTS AND DISCUSSION

3.1. Characterization of synthesized MMTCo

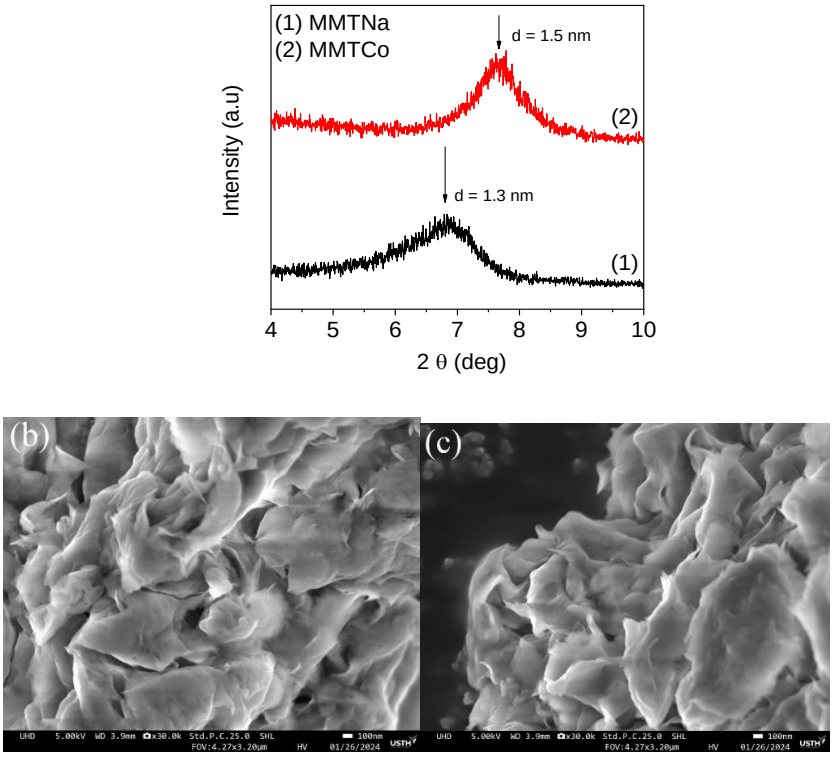

*Figure 1.*X-ray diffraction patterns of MMTNa and MMTCo (a) and FE-SEM images of MMTNa (b) and MMTCo (c) particles.

Figure 1 displays the X-ray diffraction patterns of MMTNa and MMTCo (a) and also the morphology of MMTNa (b) and MMTCo (c) determined by FE-SEM. The peak labeled d_{001} corresponds to the d-spacing in the lamellar structure of MMTNa. The d-spacing was calculated using Bragg's Law, as given in equation 1:

$$\lambda = 2d \sin\theta \quad (1)$$

where λ is the wavelength of the X-ray radiation, θ is the glancing angle, and d is the interplanar spacing of the clay platelets. From Figure 1, the calculated d-spacing (d_{001}) was 12.7 and 15.0 Å for the MMTNa and MMTCo, respectively. The change of d_{001} in the MMTCo compared to MMTNa is due to the replacement of Na^+ by Co^{2+} within the MMTNa gallery, related to the difference of the atomic radius between the sodium and cobalt ions. As the consequence, the layer spacing is increased from 12.7 to 15.0 Å also the displacement of 2θ position, as can be observed in Figure 1a. This phenomenon has been approved when observed the FE-SEM observation of MMTNa (Figure 1b) and MMTCo (Figure 1c). Compared to the morphology of MMTNa, the MMTCo nanoparticles shows not only an enlargement in inter-lamellar layer but also no accumulation. This is related to the enlargement of d-spacing when adding cobalt in the lamellar structure of MMTNa.

The release of Co from the MMTCo matrix into the aqueous solution across various pH levels was quantitatively assessed using the UV-Vis spectroscopy method. Figure 2 illustrates the Co release kinetics in both neutral and alkaline environments over time. The pH of the alkaline environment was set at 9 due to the tendency for precipitation to occur between Co^{2+} ions and OH^- ions at higher pH (pH 10). This decision was made to prevent the formation of insoluble compounds that could interfere with the accurate assessment of Co release. Although the release profiles in both conditions followed a similar pattern, their release rates varied significantly. In the alkaline medium, it occurred rapidly in the first 2 hours, and then slowed down after the next 1 hour and then remained stable during the subsequent 24 hours. The release rate of Co in the neutral solution (pH 7) initially surged during the first 4 hours, followed by a slight decline. This reduction after 4 hours could likely be due to the re-absorption of Co cations back into the matrix. The peak release rate reached approximately 45 wt.% in the neutral medium, compared to 30 wt.% in the alkaline medium.

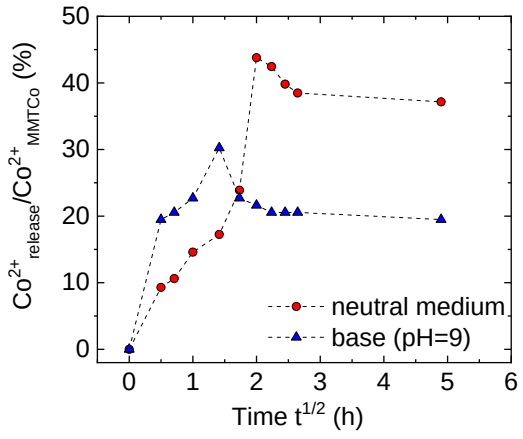

Figure 2. Co^{2+} release from MMTCo in the electrolytic solution.

The data illustrated in Figures 1 and 2 underscore the successful incorporation of Co cations within the MMTNa matrix, and MMTCo's effective release of Co into the aqueous environment. Additionally, the release dynamics were significantly affected by the pH of the medium; the process unfolded more gradually in a neutral medium and more swiftly in an alkaline setting. However, the release of Co content was higher in the neutral medium compared to the alkaline medium. This can be attributed to the precipitation of $Co(OH)_2$ in the alkaline solution.

3.2. Inhibitor efficiency of MMTCo filtrate solution

The inhibitive effect of MMTCo for AA2024 surface was evaluated using EIS method in the electrolyte with filtrate of varying MMTCo concentrations. For comparison, a reference measurement was also performed with a filtrate of 0.1 wt.% MMTNa which was neutral pH, the same condition like a filtrate extracted from 1.0 wt.% MMTCo solutions (approximately 6.5). At higher MMTNa concentrations (1.0 wt.%), the pH of the solution became alkaline (pH > 8) [11], that accelerated faster the dissolution of aluminum. The impedance measurements were conducted after 20 hours of exposure and depicted in Bode plots (Figures 3a, b) and also in Nyquist plots (Figure 3c).

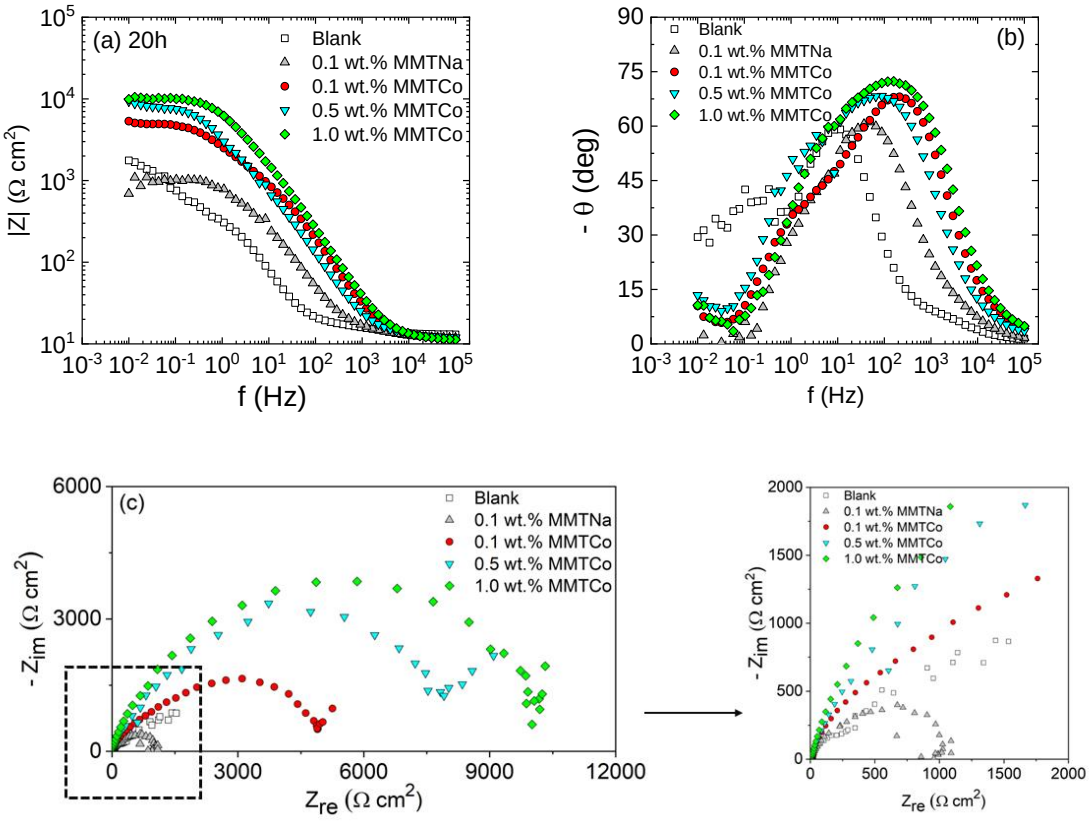

Figure 3. Electrochemical impedance diagrams (a, b) in Bode plots, (c) in Nyquist plots obtained at the E_{corr} for the AA2024 electrode after 20 hours immersed in an electrolyte containing 0.1 wt.% MMTNa and MMTCo at different concentrations.

In the blank electrolyte solution, the Bode plot reveals two time-constants: a shoulder appeared at high frequency (10^4 Hz; 10^2 Hz), attributed to the charge transfer process, and the second at a lower frequency (10^2 Hz; 10 mHz), associated with oxygen diffusion [15]. This is also corresponded with the result obtained in Nyquist plot that presented one semi-circle and a long tail of corrosion processes. For the MMTCo filtrate, regardless of the MMTCo concentration, the EIS diagrams exhibited only one time constant at a high frequency (10^4 Hz), as depicted in Figure 3b. This is also observed in Nyquist plots (Figure 3c) that presented one semi-circle and a small tail at the low frequency related to the oxygen diffusion. The modulus values increased progressively with MMTCo concentration (Figure 3a), linked to the formation of a protective film on the AA2024 surface. Moreover, the emergence of a slight tail in the very low frequency region of the diagrams indicates the diffusion of oxygen through this protective film. In contrast, the modulus value associated with the AA2024 electrode in the 0.1 wt.% MMTNa filtrate was markedly lower, signifying that the inhibitive effect is notably absent in solutions lacking Co cations. In the Nyquist plot, an inductive loop can be observed that may be indicated to the adsorption of MMTNa on the AA2024 surface resulting in the formation of a porous interlayer [16]. This distinct difference highlights the critical role of Co cations present in the filtrate in enhancing the corrosion resistance of the AA2024 surface.

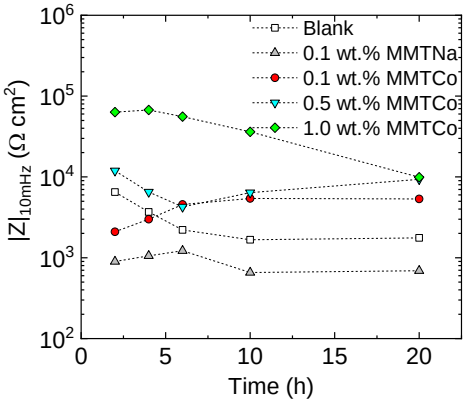

Figure 4. Variation of $|Z|_{10mHz}$ values during immersing in the filtrate solution.

The modulus values at 10 mHz ($|Z|_{10mHz}$) were extracted from the EIS diagrams over the exposure time and are reported in Figure 4. In the MMTNa filtrate, a decline in $|Z|_{10mHz}$ values over time was noted, potentially due to the solution's slightly alkaline pH (pH 8), which facilitated the corrosion reaction, progressively diminishing the impedance. In contrast, for specimens tested in the MMTCo filtrate solution, a higher concentration of MMTCo resulted in higher $|Z|_{10mHz}$ values. The most effective protection was achieved with a high concentration of MMTCo (1.0 wt.%), and this protection was maintained throughout the 20-hour test period. The results demonstrate that the release of Co^{2+} from MMTCo into the aqueous solution can effectively limit the corrosion reaction on the AA2024 surface. This finding is consistent with previous research, which also observed similar protective effects on an AA2024 electrode immersed in an aqueous solution containing low concentrations of Co^{2+} (0.001M – 0.1M) [17].

Figure 5 represents the electrochemical equivalent circuit (EEC) used to model the electrochemical behavior of all studied systems. While the R_e represents the electrolyte resistance, the EEC corresponded to the blank solution (a) shows two different part which

related to the two different electrochemical phenomenon. The R_f indicates to the resistance of the corrosion product film on the AA2024 surface; and CPE, a constant phase element that accounts for the non-ideal capacitive behavior of the film while R_{ct} is the charge transfer resistance through the film, and C_{dl} models the capacitance of the double layer at the metal-electrolyte interface. When the AA2024 electrode immersed in the electrolyte solution containing MMTNa particles, the R_{ad} component is added in the EEC (b) that related to the adsorption of nanoclay particles on the surface of AA2024 [16]. This phenomenon is visibly observed in the Nyquist plot (Figure 3c). Compared to the Bode plot and Nyquist plot obtained in the presence of MMTCo, the Warburg component (W) appears in the EEC (c) indicates to the diffusion of oxygen through the protective layer.

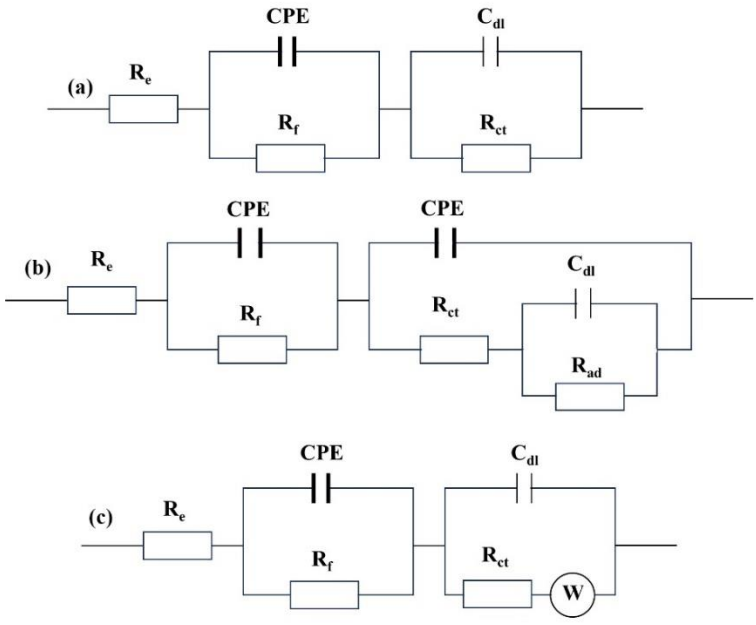

Figure 5. Equivalent electrical circuits used to fit the impedance diagrams for AA2024 electrode immersed in the blank solution (a), in the electrolyte solution contained MMTNa (b), and MMTCo (c).

From the EEC model, R_f values were identified and used to calculate the inhibitive efficiency (EI) following equation 2:

$$EI = \frac{R_f^i - R_f^w}{R_f^w} \quad (2)$$

in which: R_f^i is the R_f value obtained in the electrolyte with inhibitors and, R_f^w correspond to the R_f value in the solution without inhibitors.

Figure 6 compares the evolution of EI values over the testing period for various MMTCo concentrations. At the beginning of immersion (2 hours), lower concentrations were associated with lower EI values. However, the EI value for 0.1 wt.% MMTCo increased rapidly after 2 hours of immersion, while it rose gradually for 0.5 wt.% MMTCo, and remained high, and stable from 10 hours of testing onwards. For a high MMTCo concentration (1.0 wt.%), the EI value stayed consistently high (96 to 99 %) throughout the immersion period. After 20 hours of

immersion, the EI values for all concentrations studied were relatively high and similar, approximately ranging from 96 to 98 %, relating to the inhibition capacity of MMTCo in the electrolyte solution.

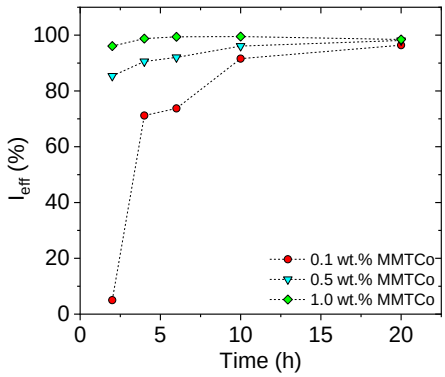

Figure 6. Variation of the inhibitive efficiency for the different inhibitors with immersion time.

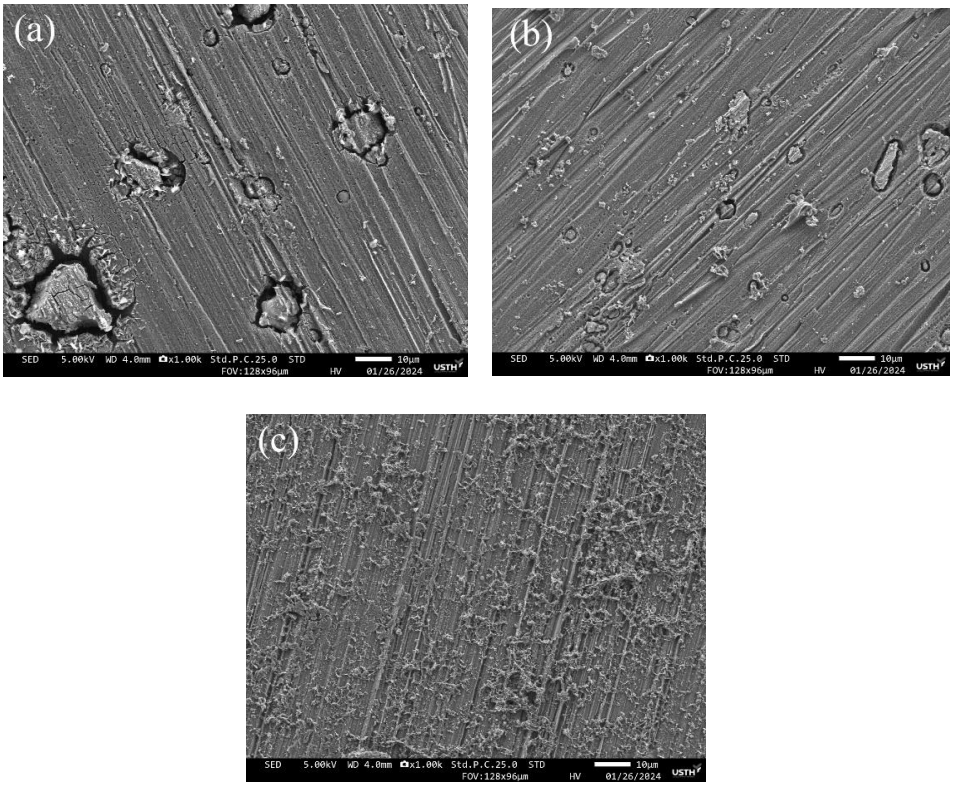

Figure 7. FE-SEM images of the AA2024 surface after 20 hours of exposure in a mixture of 0.1 M Na_2SO_4 + 0.05 M NaCl solution: (a) without MMTNa; (b) with 0.1 wt.% MMTNa and (c) with 1.0 wt.% MMTCo.

FE-SEM micrographs of the AA2024 surface following a 20-hour immersion in an electrolyte that supplemented with MMTNa at a concentration of 0.1 wt.%, and MMTCo at 1.0 wt.%, are depicted in Figure 7. In the absence of corrosion inhibitor and with the addition of

0.1wt.% MMTNa, localized corrosion is prominently visible on the surface. This is evidenced by the re-deposition of copper around the particles, manifesting as dark areas (as shown in Figures 7a and 7b), accompanied by the formation of crevices surrounding the particles.

Conversely, the specimen immersed in a solution containing 1.0 wt.% MMTCo exhibits a significant protective effect; showing no signs of corrosion on the surface. A dense layer fully encapsulates the surface, effectively shielding the intermetallic particles from galvanic corrosion. Notably, the majority of these particles appear unscathed (refer to Figure 7c). Across all samples, numerous surface cracks were observed, likely attributable to the extraction process from the solution and subsequent drying within the FE-SEM chamber. This phenomenon underscores the potential of MMTCo in the electrolyte to serve as an effective corrosion inhibitor for the AA2024 alloy.

It was documented in the literature that Co (II) salt can inhibit the corrosion of the aluminum alloy through cathode mechanism by the reaction between Co^{2+} with hydroxyl, which generated by cathode reaction equations 3 and 4 [18,19]:

$$O_2 + H_2O + 4e^- \rightarrow 4\ OH^- \quad (3)$$

$$Co^{2+} + 2OH^- \rightarrow Co(OH)_2 \quad (4)$$

In this study, MMTCo demonstrates a strong release into the neutral medium, highlighting its potential as an active inhibitor within the primer. This allows for a controllable release, particularly when the film is damaged and the cathodic reaction occurs.

4. CONCLUSIONS

MMTCo was prepared through a cation exchange reaction between $Co(NO_3)_2$ salt and montmorillonite. The synthesized MMTCo is notably extractable in aqueous environments, particularly in neutral mediums.

Electrochemical impedance spectroscopy has demonstrated that MMTCo effectively inhibits corrosion on the AA2024 surface in aqueous media. The inhibitory efficiency of MMTCo is particularly pronounced at higher concentrations. FE-SEM observations revealed that a thick and dense film formed on the AA2024 surface when exposed to the filtrate of MMTCo.

Acknowledgements. This research is funded by Vietnam National Foundation for Science and Technology Development (NAFOSTED) under grant number 104.06-2019.20

CRediT authorship contribution statement. Thai Thu Thuy: Methodology, Investigation, Writing – review & editing. Pham Gia Vu: Investigation, Validation. Trinh Anh Truc: Supervision, Conceptualization, Writing – review & editing.

Declaration of competing interest. The authors declare that they have no known competing financial interests or personal relationships that could have appeared to influence the work reported in this paper.

REFERENCES

1. Kartsonakis I. A., Athanasopoulou E., Snihirova D., Martins B., Koklioti M. A., Montemor M. F., Kordas G., Charitidis C. A. - Multifunctional epoxy coatings combining a mixture of traps and inhibitor loaded nanocontainers for corrosion protection of AA2024-T3, Corros. Sci. **85** (2014)147-159. doi.org/10.1016/j.corsci.2014.04.009.

2. Morcillo M. - Soluble salts: their effect on premature degradation of anticorrosive paints. Prog. Org. Coat., **36** (1999) 137-147. doi.org/10.1016/S0300-9440(99)00036-3.
3. Dias S.A.S., Marques A., Lamaka S.V., Simões A., Diamantino T.C., and Ferreira M.G.S. - The role of Ce(III)-enriched zeolites on the corrosion protection of AA2024-T3. Electrochim. Acta., **112** (2013) 549–556. doi.org/10.1016/j.electacta.2013.09.026
4. Balaskas A.C., Kartsonakis I.A., Tziveleka L.-A., and Kordas G.C. - Improvement of anti-corrosive properties of epoxy-coated AA2024-T3 with TiO_2 nanocontainers loaded with 8-hydroxyquinoline. Prog. Org. Coat., **74** (2012) 418–426. doi.org/10.1016/j.porgcoat.2012.01.005.
5. Kartsonakis I., Daniilidis I., and Kordas G. - Encapsulation of the corrosion inhibitor 8-hydroxyquinoline into ceria nanocontainers. J. Sol-Gel Sci. Technol., **48** (2008) 24–31. doi.org/10.1007/s10971-008-1810-4.
6. Montemor M.F. and Ferreira M.G.S. - Analytical characterization of silane films modified with cerium active nanoparticles and its relation with the corrosion protection of galvanized steel substrate. Prog. Org. Coat., **63** (2008) 330–337. doi.org/10.1016/j.porgcoat.2007.11.008
7. Sultan S., Kareem K., He L. - Synthesis, characterization and resistant performance of α-Fe_2O_3@SiO_2 composite as pigment protective coatings. Surf. Coat. Technol., **300** (2016) 42–49. doi.org/10.1016/j.surfcoat.2016.05.010.
8. Deflorian F., Rossi S., Fedel M., Motte C. - Electrochemical investigation of high-performance silane sol-gel films containing clay nanoparticles. Prog. Org. Coat., **69** (2010) 158–166. doi.org/10.1016/j.porgcoat.2010.04.007
9. Naderi R., Fedel M., Deflorian F., Poelman M., Olivier M.-G. - Synergistic effect of clay nanoparticles and cerium component on the corrosion behavior of eco-friendly silane sol-gel layer applied on pure aluminum. Surf. Coat. Technol., **224** (2013) 93–100. doi.org/10.1016/j.surfcoat.2013.03.005.
10. Motte C., Poelman M., Roobroeck A., Fedel M., Deflorian F., Olivier M.-G. - Improvement of corrosion protection offered to galvanized steel by incorporation of lanthanide modified nanoclays in silane layer. Prog. Org. Coat., **74** (2012) 326–333. doi.org/10.1016/j.porgcoat.2011.12.001
11. Thai T. T., Trinh A. T., Olivier M.-G. - Hybrid sol-gel coatings doped with cerium nanocontainers for active corrosion protection of AA2024. Prog. Org. Coat., **138** (2020) 105428.doi.org/10.1016/j.porgcoat.2019.105428.
12. Darmiani E., Danaee I., Rashed G.R., Zaarei D. - Formulation and study of corrosion prevention behavior of epoxy cerium nitrate-montmorillonite nanocomposite coated carbon steel. J. Coat. Technol. Res., **10** (4) (2013) 493–502. doi.org/10.1007/s11998-012-9463-1
13. Sturgill J.A., Phelps A.W., Swartzbaugh J.T. - Non-toxic corrosion-protection pigments based on cobalts. Patent US 7,833,331 B2.
14. Trinh Anh Truc, To Thi Xuan Hang, Vu Ke Oanh, Eric Dantras, Colette Lacabanne, Djar Oquab, Nadine Pébère. - Incorporation of an indole-3 butyric acid modified clay in epoxy resin for corrosion protection of carbon steel. Surf. Coat. Technol., **202**(20) (2008) 4945–4951. doi.org/10.1016/j.surfcoat.2008.04.092

15. Arnott D. R., Hinton B. R. W., and Ryan N. E. - Cationic-Film-Forming Inhibitors for the Protection of the Aluminum Alloy AA 7075 Against Corrosion in Aqueous Chloride Solution. Corrosion., **45** (1989) 12-18. doi.org/10.5006/1.3577880.
16. Yuanyuan Ji, Quian Hu, Da-Hai Xia, Jing-Li Luo. - Corrosion susceptibility of passive films on 1060, 2024 and 5083 aluminum alloys: experimental study and first-principles calculations. J. Electrochem. Soc., **170** (2023) 041505. doi.org/10.1149/1945-7111/accab8.
17. Thu Thuy Thai, Anh Truc Trinh, Gia Vu Pham, Thi Thanh Tam Pham, Hoan Nguyen Xuan. - Corrosion protection properties of cobalt salt for water-based epoxy coatings on 2024-T3 aluminum alloy. Corros. Sci. Technol., **19** (1) (2020) 8-15. doi.org/10.14773/cst.2020.19.1.8
18. Henry Leidheiser, Jr. and Ichiro Suzuki. - Cobalt and Nickel Cations as Corrosion Inhibitors for Galvanized Steel. J. Electrochem. Soc., **128** (2) (1981) 242. doi.org/10.1149/1.2127399.
19. Henry Leidheiser, Jr. and Gary W. Simmons. - Mössbauer Spectroscopic Study of the Corrosion Inhibition of Zinc by Cobalt Ions. J. Electrochem. Soc., **129** (8), (1982)1658. doi.org/10.1149/1.2124231.